Journal of Soils and Sediments
https://doi.org/10.1007/s11368-018-02223-0

SEDIMENTS, SEC 3 • HILLSLOPE AND RIVER BASIN SEDIMENT DYNAMICS • RESEARCH ARTICLE

Coupling hysteresis analysis with sediment and hydrological connectivity in three agricultural catchments in Navarre, Spain

Saskia D. Keesstra[1,2] · Jason Davis[3] · Rens Hein Masselink[3] · Javier Casalí[4] · Edwin T. H. M. Peeters[5] · Roel Dijksma[6]

Received: 18 May 2018 / Accepted: 16 December 2018

Abstract

Purpose Rain storm events mobilise large proportions of fine sediments in catchment systems. Sediments from agricultural catchments are often adsorbed by nutrients, heavy metals and other (in)organic pollutants that may impact downstream environments. To mitigate erosion, sediment transport and associated pollutant transport, it is crucial to know the origin of the sediment that is found in the drainage system, and therefore, it is important to understand catchment sediment dynamics throughout the continuity of runoff events.

Materials and methods To assess the impact of the state of a catchment on the transport of fine suspended sediment to catchment outlets, an algorithm has been developed which classifies rain storm events into simple (clockwise, counter-clockwise) and compound (figure-of-eight; complex) events. This algorithm is the first tool that uses all available discharge and suspended sediment data and analyses these data automatically. A total of 797 runoff events from three experimental watersheds in Navarre (Spain) were analysed with the help of long-term, high-resolution discharge and sediment data that was collected between 2000 and 2014.

Results and discussion Morphological complexity and in-stream vegetation structures acted as disconnecting landscape features which caused storage of sediment along the transport cascade. The occurrence of sediment storage along transport paths was therefore responsible for clockwise hysteresis due to the availability of in-stream sediment which could cause the "first flush" affect. Conversely, the catchment with steeper channel gradients and a lower stream density showed much more counter-clockwise hysteresis due to better downstream and lateral surface hydrological connectivity. In this research, hydrological connectivity is defined as the actual and potential transfer paths in a catchment. The classification of event SSC-Q hysteresis provided a seasonal benchmark value to which catchment managers can compare runoff events in order to understand the origin and locations of suspended sediment in the catchment.

Conclusions A new algorithm uses all available discharge and suspended sediment data to assess catchment sediment dynamics. From these analyses, the catchment connectivity can be assessed which is useful to develop catchment land management.

Keywords Headwater catchment · Hydrological event · Hysteresis · Sediment connectivity · Sediment dynamics

Responsible editor: Nikolaus Kuhn

✉ Saskia D. Keesstra
saskia.keesstra@wur.nl

[1] Team Soil Water and Land Use, Wageningen Environmental Research, Wageningen UR, P.O. Box 47, 6700 AA Wageningen, The Netherlands

[2] Civil, Surveying and Environmental Engineering, The University of Newcastle, Callaghan 2308, Australia

[3] Soil Physics and Land Management Group, Wageningen University, Droevendaalsesteeg 4, 6708 PB Wageningen, The Netherlands

[4] Department of Engineering, Public University of Navarre, Campus Arrosadía, 31006 Pamplona, Spain

[5] Aquatic Ecology and Water Quality Management Group, Wageningen University, Droevendaalsesteeg 4, 6708 PB Wageningen, The Netherlands

[6] Department of Hydrology and Quantitative Water Management, Wageningen University, Droevendaalsesteeg 4, 6708 PB Wageningen, Netherlands

Published online: 04 January 2019

1 Introduction

Increased sediment loads, adsorbed with nutrients, heavy metals and other organic and inorganic pollutants, impact downstream aquatic ecological environments (Owens and Walling 2002; Bilotta and Brazier 2008; Bird et al. 2010; Song et al. 2011; Kjelland et al. 2015). In Mediterranean areas, soil erosion by water is particularly problematic due to the climatic, pedological and geomorphological conditions (Cerdan et al. 2010; García-Ruiz et al. 2013). Long-term, high temporally resolute data on precipitation, runoff and water turbidity have provided the data to study trends in precipitation, runoff and suspended sediment production (e.g. Casalí et al. 2008). However, when flow and sediment measurements are confined to catchment outlet, it has been proven to be difficult to consistently define relationships between runoff data and the physical processes occurring at the catchment scale (Stubblefield et al. 2007) which are known to be conditioned by topography, infiltration dynamics, climate, channel pattern, vegetation, land use and soil properties (Roehl 1962). Based on initial catchment conditions such as soil moisture, vegetation density, soil erodibility, and (dis)connective landscape features, sediment production, transfer and storage may be controlled by all parts of the landscape (Parsons et al. 2006; Wainwright et al. 2011; Bracken et al. 2015; Cerdà et al. 2017). Subsequently, each location in the catchment has a temporally dynamic influence on both discharge (Q) and suspended sediment concentration (SSC) measured at the outlet. Hydrograph and suspended sediment time-series analysis have revealed patterns from which the activation and location of runoff generation and sediment transport processes can be inferred by classifying hydrological events based on the disparity between the time-to-peak of the hydrograph and sediment time series.

Suspended sediment hysteresis is a term that describes the nonlinear relationship between SSC and Q during a discharge wave (Klein 1984; Gentile et al. 2010). The array of coordinate points generated by plotting SSC vs. Q through time forms a loop figure (hysteresis loop) whose size, direction and shape reflect the lag in response between SSC and Q (Seeger et al. 2004). This loop figure has been studied using a technique called hysteresis analysis, in which the type and location of physical processes leading to runoff generation and sediment transport are hypothesised to be explanatory factors for the event loop direction and shape (Gao and Josefson 2012; Aich et al. 2014). SSC-Q hysteresis loop examination has thereby allowed for the inferencing of major sediment source areas which are regarded to contribute to sediment transport cascade in catchments (Keesstra et al. 2009; Ziegler et al. 2014). Clockwise loops (CW; with Q on the x-axis and SSC on the y-axis) result from the main SSC peak pre-empting Q peak. In terms of process, this type of curve indicates that sediment is primarily originated from, in or nearby stream channels in the lower part of the catchment (Seeger et al. 2004). It signals the flushing of highly erodible sediment which was deposited from up-catchment locations during prior storm events (Jansson 2002; Wotling and Bouvier 2002; Rovira and Batalla 2006; Gao and Pasternack 2007; Gao and Josefson 2012). Counter-clockwise (CCW) loops result from Q peaking before the SSC. CCW loops may signal distal sediment supply, delayed in-channel sediment resuspension caused by the late break-up of biofilms, in-channel (bank erosion) sediment sources, or intra-storm variable rainfall patterns (Lawler et al. 2006; López-Tarazón et al. 2009; Mano et al. 2009). A more complex figure-eight loop results from secondary peaks in Q or SSC. This type of loop could signal intra-catchment transport of suspended sediment of heterogeneous sizes (Smith and Dragovich 2009) or a combination of different runoff generation processes (Zabaleta et al. 2007).

Insofar as it describes catchment runoff and sediment dynamics, hysteresis analysis has evolved from a qualitative classification system into a data-intensive, quantitative technique. In observing single flood events, Williams (1989) and Klein (1984) provided qualitative explanations of the hysteresis loop phenomenon. Subsequent studies in headwater catchments classified events by the loop type (e.g. Regüés et al. 2000) and linked event loop types to observed physical processes. However, most of these studies lacked quantitative data which could consistently explain loop directions using statistical models and were unable definitively elaborate on the factors controlling runoff generation. Seeger et al. (2004), in a year-long study in the Central Spanish Pyrenees, not only classified storm events by loop type, but also applied a multivariate analysis in the form of a canonical discriminant analysis to resolve and isolate the combinations of initial physical conditions, such as soil moisture content and antecedent precipitation indices, and ultimately link them to classified loop types. Other studies developed hysteresis indexes which could systemically classify loop direction (the hysteresis index, HI) (Langlois et al. 2005; Lawler et al. 2006: Lloyd et al. 2016), and thus made it possible for quantitative, comparative studies both within and across multiple catchments. In a comparative catchment study, Sherriff et al. (2015) applied a principal component analysis in conjunction with the HI metric to graphically and analytically explain the various factors influencing catchment sediment dynamics.

SSC-Q hysteresis analysis can play a role in explaining catchment sediment dynamics under conditions of full data inclusion and use of robust loop analysis methods (Sith et al. 2017). However, further improvements can be made which can fully automate the procedure for loop direction and event type classification. Additional knowledge can be garnered by increasing the relevant data inputs and employing multivariate statistical models which can link event types to a complex set of explanatory data on initial catchment conditions as well as discharge and precipitation variables (Lloyd et al. 2016). The

combination of these techniques could greatly improve the understanding of event sediment dynamics by isolating the most important and explanatory event and climatic variables. This presents an opportunity for geomorphological understanding and sediment production in headwater catchments. Therefore, the main aim of this research is to assess the runoff and erosion dynamics in three small Mediterranean catchments (area < 6 km^2) by classifying runoff events by the type of hysteresis and linking these groups to the respective catchment characteristic data and event runoff variables. From this analysis, the application potential and robustness of this new methodology was assessed.

2 Materials and methods

2.1 Study areas

The data in this study come from three catchments in the Navarre region, in Northern Spain (Fig. 1). They are part of a network of experimental research catchments instituted to assess erosion, nutrient transport and hydrological processes within agricultural and semi-natural landscapes (Casalí et al. 2010; Masselink et al. 2016). Catchments were selected based on data availability as well as due to the major differences in land use and cover (Masselink et al. 2016). This made it possible to assess the relevance of different environmental variables on runoff and sediment production. The Latxaga (2.07 km^2) and La Tejería (1.69 km^2) catchments' land use is dominated by rain-fed agricultural fields (90%) mostly covered with winter wheat (*Triticum aestivum*), barley (*Hordeum vulgare*) and sometimes legumes (*Vicia faba* L. and *Pisum sativum* L.) or sunflower (*Helianthus annus* L.). However, the stream beds and banks within the La Tejería watershed are poorly vegetated, which enhances the occurrence of bank erosion processes. The Oskotz (5.05 km^2) experimental catchment contains nearly 100% forest cover mainly composed of *Fagus sylvatica, Quercus pyrenaica* and *Pinus* spp. It is more humid and has a lower runoff coefficient (Casalí et al. 2012) than both agricultural catchments. The Latxaga and La Tejería watersheds both have humid sub-Mediterranean climates, with average annual precipitations of 835 and 725 mm, distributed over 95–100 and 105 rainfall days and average annual temperatures of 12 °C and 13 °C, respectively. Geologically, these two catchments are underlined by clay marls and grey marls. La Tejería contains sandstones of continental facies. Because of the soft nature of the lithology, the sediment yield at the outlet of the catchments consists mainly of suspended sediment. Almost all coarser material has been broken into small sized particles before reaching the outlet of the catchments. Oskotz watershed has a sub-Atlantic climate, with an average annual precipitation of 1242 mm, distributed over 130 rainfall days, and an average annual temperature of 12 °C. Detailed climate and catchment environmental properties are shown in Table 1.

2.2 Data collection and data treatment

Rainfall was recorded using a tipping bucket device with 0.2 mm resolution with every tip of the device. Additionally, each catchment had at the watershed outlet one hydrology station from which water level (mm) and turbidity (NTU) were recorded every 10 min. The discharge measurement device consisted of a triangular profile flat-V weir which allowed sediment to pass the control section; discharge ($m^3\ s^{-1}$) was calculated from water level data which was gathered using a pressure probe and this was verified with a direct measurement propeller-type current meter and triangular and rectangular sharp-crested weirs. To isolate effects of total rainfall, intensity and duration, a rainfall event erosivity index based on kinetic energy (KE; MJ $ha^{-1}\ mm^{-1}$) of the event precipitation was derived (Morgan 2005). Kinetic energy was calculated according to Cerro et al. (1998). The empirical relationship for KE was based on rain drop size distributions and was derived from regions of similar climatic conditions. Given climatic similarities, the relationship was seen as most representative for the three catchments in this study. Thus, kinetic energy was calculated as follows (Cerro et al. 1998):

$$KE = 0.384*\left(1-.54e^{-0.029*I_{60}}\right) \quad (1)$$

Where: I_{60} is the 60-min rainfall intensity (mm h^{-1}). An event's total kinetic energy was calculated from:

$$KE_{\text{total}} = \sum_{t=0}^{\text{Dur}} E_t * P_{\text{total}} \quad (2)$$

Where t was the time step, E_t was the kinetic energy for each time step and P_{total} was the total rainfall received at time step t. Finally, the EI_{30} was calculated as:

$$EI_{30} = KE_{\text{total}} * I_{30} \quad (3)$$

Where I_{30} was the maximum 30-min rainfall intensity in mm h^{-1}. For I_{60} intensities above 76 mm h^{-1}, a maximum I_{60} was used according to (Brown and Foster 1987). The Antecedent Precipitation Index (Linsley and Kohler 1951) was used as a surrogate of soil moisture in this study:

$$\text{API} = \sum_{t=0}^{i} P_t * k^{-1} \quad (4)$$

Where API is Antecedent Precipitation Index (mm), P_t the precipitation on day t (mm), k a calibration factor and t is the number of days before $t = 0$. The model for antecedent

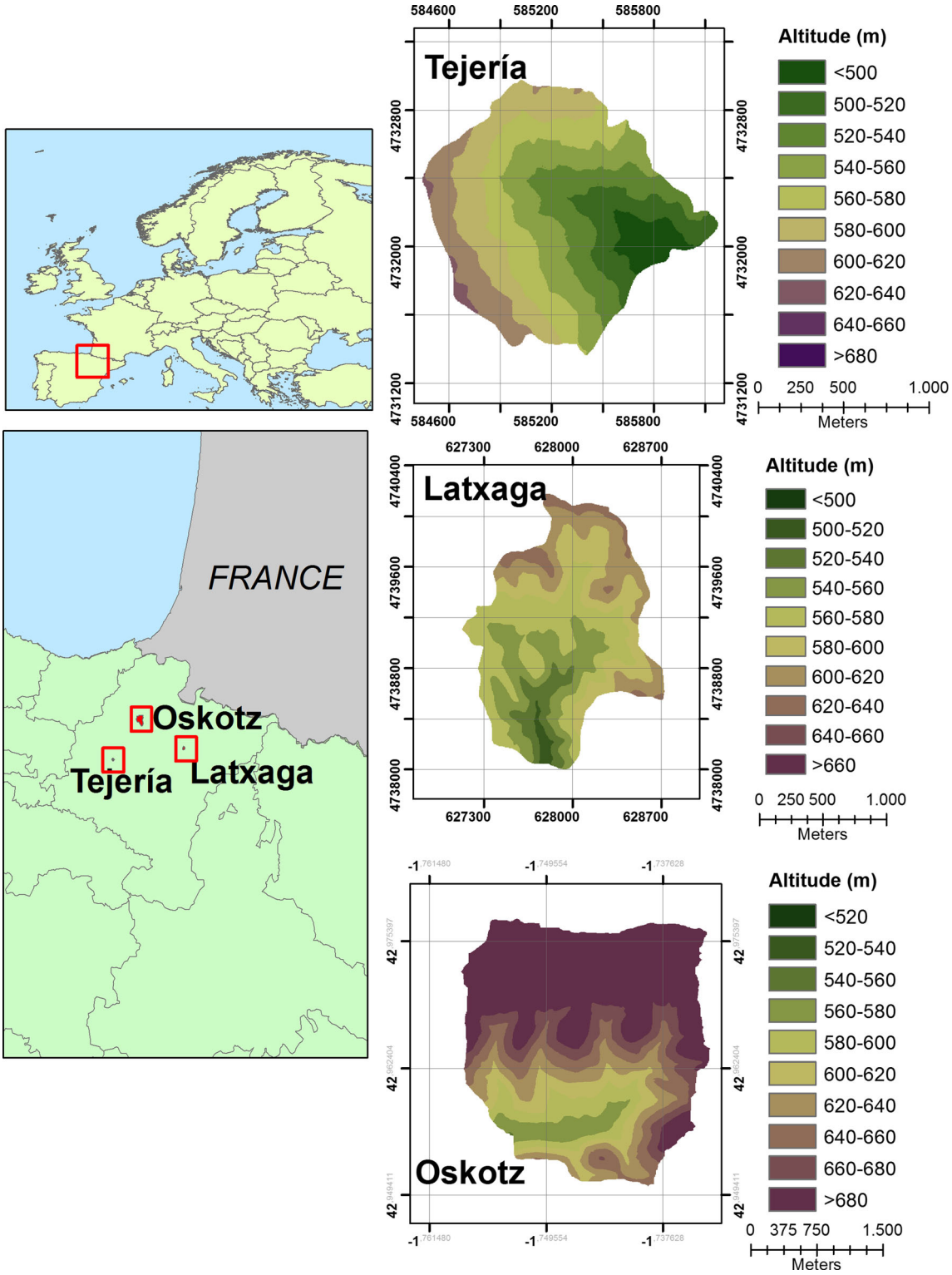

Fig. 1 Study area: Latxaga, La Tejería and Oskotz watersheds are part of the experimental agricultural watershed network of the Government of Navarre

precipitation was calibrated according to Masselink et al. (2016). Finally, changes in vegetation cover were captured using the Normalised Difference Vegetation Index (NDVI; Dash et al. 2007) and it was used in this study as an indicator for crop maturity and vegetation growth. It was calculated using satellite imagery as:

Table 1 Catchment environmental characteristics

	Latxaga	Tejeria	Oskotz
Location	42° 47′ 7.5″ N 1° 26′ 11.4″ W	42° 44′ 710.6″ N 1° 56′ 57.2″ W	42° 57′ 29.14″ N 1° 46′ 43.58″ W
Area (km^2)	2.07	1.69	5.05
Perimeter (km)	6.67	5.46	11.44
Total channel length km)	5.38	3.2	7.41
Minimum elevation (m)	504	496	539
Maximum elevation (m)	639	649	792
Av slope (%)	19.3	14.8	19.8
Av. (permanent) channel slope (%)	12.4	14.6	5.1
Climate	Humid submediterranean	Humid submediterranean	Sub-Atlantic
Annual precipitation (mm)	835	725	1242
Rainfall days	100	105	130
Av. Temperature °C	12	13	12
Lithology	Marls, grey marls	Marls, sandstones	Marls
Gravelius index	1.30	1.17	0.92
Shape Factor	0.26	0.54	0.37
Drainage density (km km2)	2.61	1.91	1.94

$$NDVI = \frac{\text{NIR}-\text{RED}}{\text{NIR} + \text{RED}} \quad (5)$$

Where: NDVI is the Normalised Difference Vegetation Index, NIR the top of atmosphere reflectance in the near-infrared wavelength bands and RED the top of the atmosphere reflectance in the red wavelength band (Masselink et al. 2016).

2.3 Storm event separation and hysteresis index calculation

Base flow was separated from event (quick) flow by applying a low-pass, recursive digital filtering algorithm to the continuous hydrograph time series according to Eckhardt (2005). The filter considers an exponential base flow recession during periods without groundwater recharge. The separation method requires two parameters: a recession constant, or filtering parameter (*a)* and a base flow index maximum (BFI_{max}). Recession analysis determined the filtering parameter by constructing a master recession curve and using the matching strip method (e.g. Nathan and McMahon 1990). BFI_{max} was determined using an empirically derived value which corresponded to classes of catchments containing hydrological and hydrogeological characteristics (Table 2).

Table 2 Base flow separation model filter constants by catchments

Catchment	a	BFI_{max}	Flow regime	Aquifer porosity
Latxaga	0.963	0.50	Ephemeral	Porous
La Tejería	0.963	0.50	Ephemeral	Porous
Oskotz	0.963	0.50	Ephemeral	Porous

An analytic definition for a runoff event allowed for a consistent definition of an 'event' over the time period. This made it possible to compare across catchments and between storms. A storm was defined as a 10% rise in quick flow above base flow. Base flow was calculated using the Local Minimum Method (Sloto and Crouse 1996). Each event ended when quick flow dropped below the calculated base flow. Consequently, it was possible to have runoff events with multiple peaks if quick flow stayed greater than base flow. To remove the influence of initial base flow conditions on the HI calculation—in order to focus on the relative changes in each variable—the turbidity and quick flow event time series for quick were normalised according to the following equations from Lloyd et al. (2015):

$$\text{Normalized } Q\text{i} = \frac{Q\text{i}-Q\text{min}}{Q\text{max}-Q\text{min}} \quad (5)$$

$$\text{Normalized } T\text{i} \frac{T\text{i}-T\text{min}}{T\text{max}-T\text{min}} \quad (6)$$

Where: Q_i/T_i is the discharge ($l\ s^{-1}$)/turbidity(NTU) at time step i, Q_{min}/T_{min} is the minimum storm parameter value and Q_{max}/T_{max} is the maximum storm parameter value. The hysteresis index was then calculated as:

$$\text{HI} = T_{\text{RL\_Qi}} - T_{\text{FL-Qi}} \quad (7)$$

Where: HI is the index at percentile i of the discharge (Q), T_{RL_Qi} is the turbidity value on the rising limb at percentile *i* of Q and T_{FL_Qi} is the turbidity value at the equivalent point in discharge on the falling limb. The percentiles of discharge (Q_i)

were defined by:

$$Q_i = k(Q_{max} - Q_{min}) + Q_{max} \quad (8)$$

Where: Q_{max} is the peak discharge (l s^{-1}), Q_{min} is the discharge at the start (l s^{-1}) of the event and k is the point along the loop where the calculation is being made. The index was calculated at every 5% of the discharge, making $k = 0.05$, 0.10...1.0 and always produced an HI value between − 1 and 1. The sign indicates clockwise versus counter clockwise and the size of the index indicates the strength of the hysteresis, or the width of the loop for the given k discharge range being measured. Each event thus contained an array of *HI* values, from which the average HI was calculated by taking the average of the array values (Lloyd et al. 2015). Figure 2 shows a model example of CW and CCW events. Time-series curves are identical but are separated slightly in time which produces the hysteresis curve.

To characterise the catchments in an objective way, we have calculated two indices: the Gravelius Index and the shape factor. The Gravelius index (K_c) has been defined as:

$$K_c = 0.28P/A^{0.5} \quad (9)$$

Where P is the catchment perimeter (m) and A the area (m^2). A perfect circular catchment would have a Kc equal to 1 (Bendjoudi and Hubert 2002) "In order to characterise the morphology of the watersheds, two indices (Gravelius Index and shape factor) were used.

The shape factor K_f has been defined by Monsalve Saenz (1999) as:

$$K_f = A/L^2 \quad (10)$$

Where P is the catchment parameter and L is the maximum length along the main stream from the catchment outlet to the most distant ridge on the drainage divide.

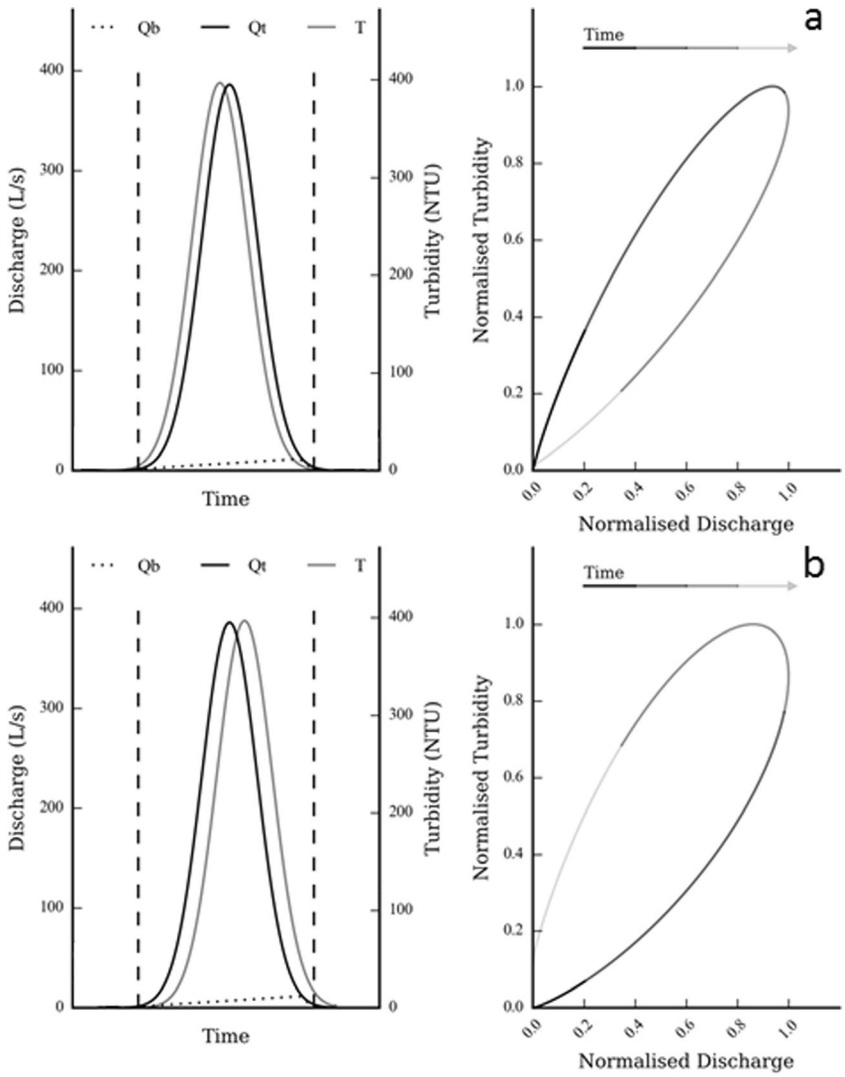

Fig. 2 **a** Example (model) storm of a clockwise hysteresis where turbidity peaks before discharge and **b** model of a counter-clockwise hysteresis event where turbidity peaks after discharge

2.4 Event type classification

While the event average HI was descriptive of the general behaviour of the event hydrograph and turbidity time series, it failed to account for intra-storm changes in loop direction, especially mid-storm loop direction reversals. Often events begin as simple hysteresis events (CW; CCW) and thereafter, due to late peaks or drops in either discharge or turbidity, appear as a figure-of-eight or complex loop. An event might begin as a simple CW loop due to an early turbidity response relative to discharge. Low magnitude spikes in either the discharge or turbidity curves would ensure the loop remains CW. If, however, a large spike in turbidity were to occur on the falling limb of the event's hydrograph, the loop would more likely resemble a figure-of-eight pattern. To capture these intra-storm periodic differences in the sign of HI, we developed a classification algorithm which differentiated between simple and complex events while still maintaining the composite loop directions from each time period, especially the starting and ending loop directions. To do this, we subdivided the event HI array into four equal time periods then computed the average HI for each quartile. An HI quartile was considered CW where $HI > 0$ and CCW where $HI < 0$. We then passed this sequence of values through a function which, based on these sign of the HI in the given range, classified each storm into one of four types (Table 3).

Table 3 Event type separation procedure based on sign of HI value calculated for each discharge quartile

Event type code	$Grouping_1$	$Grouping_2$	HI_{q1}	HI_{q2}	HI_{q3}	HI_{q4}
1	CW	CW	+	+	+	+
2	CW	CW	+	+	+	–
3	CW	Figure-of-eight	+	+	–	–
4	CW	Figure-of-eight	+	+	–	+
5	CCW	CCW	+	–	–	–
6	CW	Figure-of-eight	+	–	–	+
7	CW	Complex	+	–	+	+
8	CW	Complex	+	–	+	–
9	CCW	CCW	–	–	–	–
10	CCW	CCW	–	–	–	+
11	CCW	Figure-of-eight	–	–	+	+
12	CCW	Figure-of-eight	–	–	+	–
13	CW	CW	–	+	+	+
14	CCW	Figure-of-eight	–	+	+	–
15	CCW	Complex	–	+	–	+
16	CCW	Complex	–	+	–	–

2.5 Statistical analyses and procedures to determine event type controls

A number of statistical analysis procedures were performed to investigate controls on hydrological response and event sediment dynamics in each watershed over the course of the study. All variable values were considered as samples from a population. Thus, the central limit theorem was assumed. One-way ANOVA was performed to infer significant differences between sampled event storm variables. When more than two groups were incorporated into an ANOVA and significant variation was found in the model, a Tukey post hoc test was conducted with $\alpha = 0.01$. In some cases, the sample size of the complex and figure-of-eight events was not large enough to include these events in the analysis. The sign of HI was then used to divide the groups into two categories, CW with $HI > 0$ or CCW with $HI < 0$. A one-tailed heterogeneous t-test for variance was then applied to confirm the presence of significant differences between the sampled variable. Finally, for each catchment, canonical variate analysis (CVA) was performed with the Canoco-5 software package (Ter Braak and Smilauer 2012) with the event types as groups and with the variables described in Table 4. These variables were therefore considered discriminating variables. In this study, CVA was used to find the best linear separation of event type samples using the discriminating variables in Table 4. In order to include only the significantly deviating variables in each catchment CVA, a procedure called forward selection was used. In this procedure, discriminating variables considered on a step-by-step basis and were only included in the model if p values were less than 0.05. This had many advantages because each time a new variable was included in the model, the p values of all non-included variables were updated. The final model included only the variables which were able to discriminate between event types. Each catchment contained a different set of diversifying variables which was able to maximise the difference between event types when viewed in canonical space.

3 Results

3.1 Event type distribution

In total, 797 storms were identified and analysed for the three catchments between 2000 and 2014. Each catchment displayed CW, CCW, figure-of-eight and complex events (Table 5). Hydrological events began under a range of initial base flow conditions. The separating function made clear distinctions between events based on the relation between base flow and quick flow; however, some events could also have been considered sub-events as they were merely peaks which

Table 4 Runoff event variables and descriptions

Runoff event parameters	
Rainfall variables	Event discharge and turbidity variables
Total precipitation, P_{total} (mm)	Time elapsed since last runoff event, T_{LE} (hours)
Event duration, duration (hours)	Baseflow at the start of event, Q_b (L s^{-1})
Antecedent precipitation index 7 days before event, API (mm)	Mean stream discharge, Q_{mean} (L s^{-1})
Maximum averaged 30 min rainfall, P_{30max} (mm)	Maximum/peak stream discharge Q_{max} (L s^{-1})
Maximum averaged 60 min rainfall, P_{60max} (mm)	Minimum stream discharge Q_{min} (L s^{-1})
Maximum averaged 120 min rainfall, P_{120max} (mm)	Range of stream discharge Q_{range} (L s^{-1})
30 min rainfall intesnity, I_{30} (mm)	Maximum stream discharge from previos storm, $Q_{max(s-1)}$ (L s^{-1})
60 min rainfall intesnity, I_{60} (mm)	Minimum stream discharge from previous storm, $Q_{min(s-1)}$ (L s^{-1})
Rainfall erosivity, EI_{30} (MJ mm^{-1} ha^{-1} h^{-1})	Range of stream discharge previous storm $Q_{range(s-1)}$ (L s^{-1})
Turbidity/suspended sediment variables	Other variables
Average turbidity, T_{mean} (NTU)	Normalised difference vegetation index, NDVI (−-)
Maximum turbidity, T_{max} (NTU)	
Minimum turbidity, T_{min} (NTU)	
Range of turbidity, T_{range} (NTU)	
Maximum turbidity previous storm, $T_{max(s-1)}$ (NTU)	
Minimum turbidity, $T_{min(s-1)}$ (NTU)	
Range of turbidity previous storm, $T_{range(s-1)}$ (NTU)	

were located on the rising or falling limb of a larger event. CW and CCW (simple event types) contained hysteresis index (HI) values for all ranges of discharge which were either positive (CW) or negative (CCW). Examples of event types are shown in Fig. 3. The CW type event was the most common and CCW events were second in frequency of occurrence. In Oskotz, CW event frequency was three times that of CCW; Latxaga had about twice as many CW events as CCW events; and La Tejería contained nearly the same amount of CW as CCW events. Compound events (complex, figure-of-eight) occurred when a simple event's main peak was preceded by or followed by a secondary (smaller) peak in either discharge or turbidity. Figure-of-eight events consisted of at least one secondary peak in turbidity or discharge that was independent from—or not in sync—with the primary discharge peak. In some cases, the secondary peak was turbidity and came before the main discharge peak. In other cases, the secondary turbidity peak appeared after the main discharge peak. Alternatively, the same event type could have resulted from a storm event having independent, secondary peaks in discharge instead of turbidity. Complex events occurred in two main contexts: first, some resulted from an event having multiple, non-synchronised peaks in both discharge and turbidity. Otherwise, they could have occurred due to volatile fluctuations in turbidity during a relatively constant base flow recession periods.

Table 5 Total recorded event type for each catchment

Catchment	CW	CCW	Fig8	Complex	Total
Latxaga	137	60	17	4	218
OskotzF	242	74	44	13	373
Tejeria	81	80	32	13	206
Total	460	214	90	35	797

3.2 Seasonal trends in hysteresis index

Variation in HI showed slightly different seasonal trends in the different watersheds (Fig. 4). In all three catchments, the average monthly HI (HI_m) gradually decreased from the period November to June. In the more elongated, less-well drained agricultural catchment of Latxaga, a positive HI_m coincided with heavier rains and lower ground cover. The greatest variation in HI for this catchment occurred in September and October and the least variation occurred as the rains became more infrequent (May–June). The Latxaga HI_m drops below zero in March, 1 month later than in La Tejería. In La Tejería, variation in HI was quite low at the seasonal onset of rains in September and increased through April. Both catchments show steeper declines in HI_m in the period February–April as compared with November–February. In contrast to both agricultural catchments, the forested catchment Oskotz showed most HI variation in February and March. Interestingly, among the three catchments, the HI_m in Oskotz fluctuated the least throughout the year.

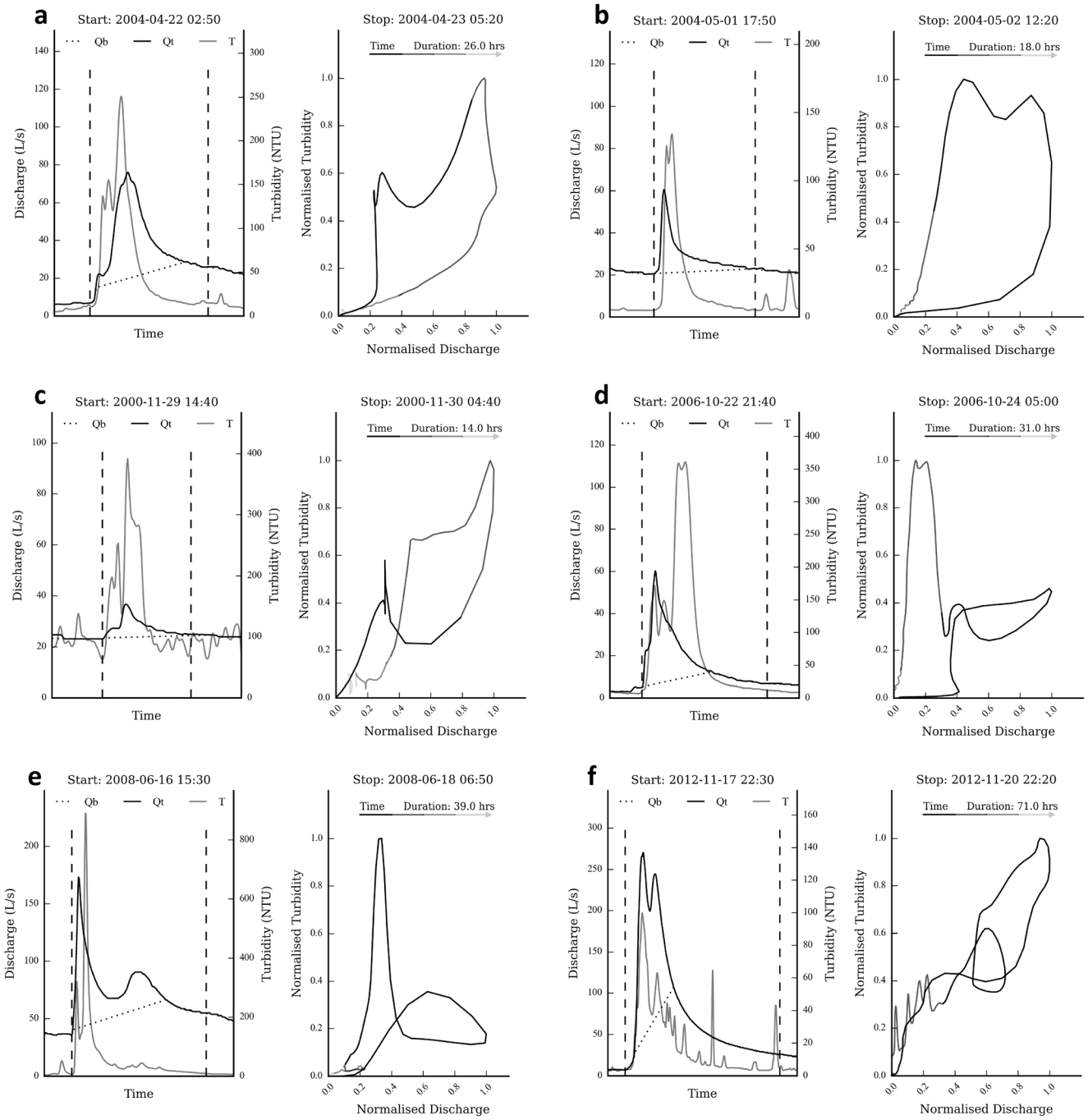

Fig. 3 Plots showing temporal hydrograph and turbidity graphs as well as hysteresis plots **a** CW—Latxaga; **b** CCW—Latxaga; **c** CW-Eight—La Tejería; **d** CCW-Eight—Oskotz; **e** CCW-Complex—Oskotz; **f** CW-Complex—Oskotz. The vertical dashed lines mark the start and stop times for each event

3.3 Variable controls on event type

Canonical variate analysis (CVA) revealed that for each catchment a different combination of discharge, precipitation or vegetation-related variables were most associated with each event type (Fig. 5, Table 6).

For Latxaga, the first canonical axis (a1) explained 85.5% of the variance between event types and was loaded by the four variables P_{total}, Duration, the turbidity range of the previous storm $T_{range(s-1)}$ and the discharge max of the previous storm $Q_{max(s-1)}$. Based on centroid locations of event groupings, this axis primarily differentiated CW from CCW and figure-of-eight events. CW events tended to receive more rain during the event itself (high P_{total}), were of long Duration and occurred after events with low discharge maximums $Q_{max(s-1)}$ and/or $T_{range(s-1)}$. Analysis of variance (ANOVA; Table 7)

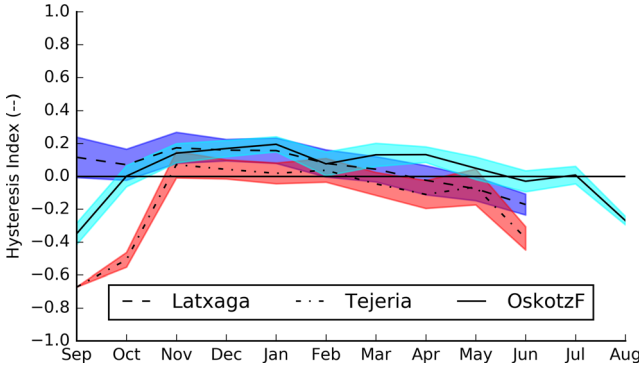

Fig. 4 Average monthly HI values plus monthly HI standard deviation

confirmed significant differences in group means for Duration ($p = 2.93e\text{-}3$), $Q_{max(s-1)}$ ($p = 2.23e\text{-}2$) and $T_{range(s-1)}$ ($p = 4.03e\text{-}2$). A post hoc Tukey test confirmed that CW events were longer than CCW in Duration and had lower values for $Q_{max(s-1)}$ ($\alpha = 0.01$) and $T_{range(s-1)}$. Lack of adequate sample size for complex events ($n = 4$) prevented any meaningful statistical analysis involving complex events. However, it is interesting to note that one complex event which occurred on 2012-10-20 had the highest P_{total} (75.32 mm) of all events in Latxaga. The second canonical axis (a2) was loaded by rainfall erosivity EI_{30} and $T_{max,}$ though this axis explained only 10% of the variation between storm types. The centroid of the CCW and figure-of-eight events were similar in a1 but were farther apart in a2, suggesting that events that started off as CCW were likely converted to figure-of-eight events due to late peaks in turbidity.

La Tejería rainfall variables exerted greater control on event type outcome than discharge variables (Fig. 4b). $Q_{mean,}$ and Q_{max} showed little variation between event types. The first canonical discriminant axis (a1) explained 84.4% of the variance and was most loaded by 30-min rainfall intensity (I_{30}) and Duration. Just three variables were significantly able to discriminate between the event types as compared with Latxaga and Oskotz, where four and five variables, respectively, could discriminate between event groupings. Total explained variance was not affected (Table 5). CCW events were shorter in Duration and occurred under higher rainfall intensities than CW events (Fig. 4b). ANOVA and post hoc Tukey tests confirmed significant variation between the simple event types in mean I_{30} ($p = 1.70e\text{-}3$), Duration (1.92e-05). Post hoc Tukey test also confirmed figure-of-eight events were significantly longer than CCW events. Additionally, of the 41 figure-of-eight events from this catchment, 34 began as CW and were later converted to figure-of-eight. API loaded the second canonical discriminant axis (a2). High I_{30} and high API caused simple CCW events to become a figure-of-eight. In contrast to the other two catchments, P_{total} did not differ between the simple event types. However, rainfall in the 6 h prior to an event (P_{06}) was greater for CCW than CW events (2.93E-02).

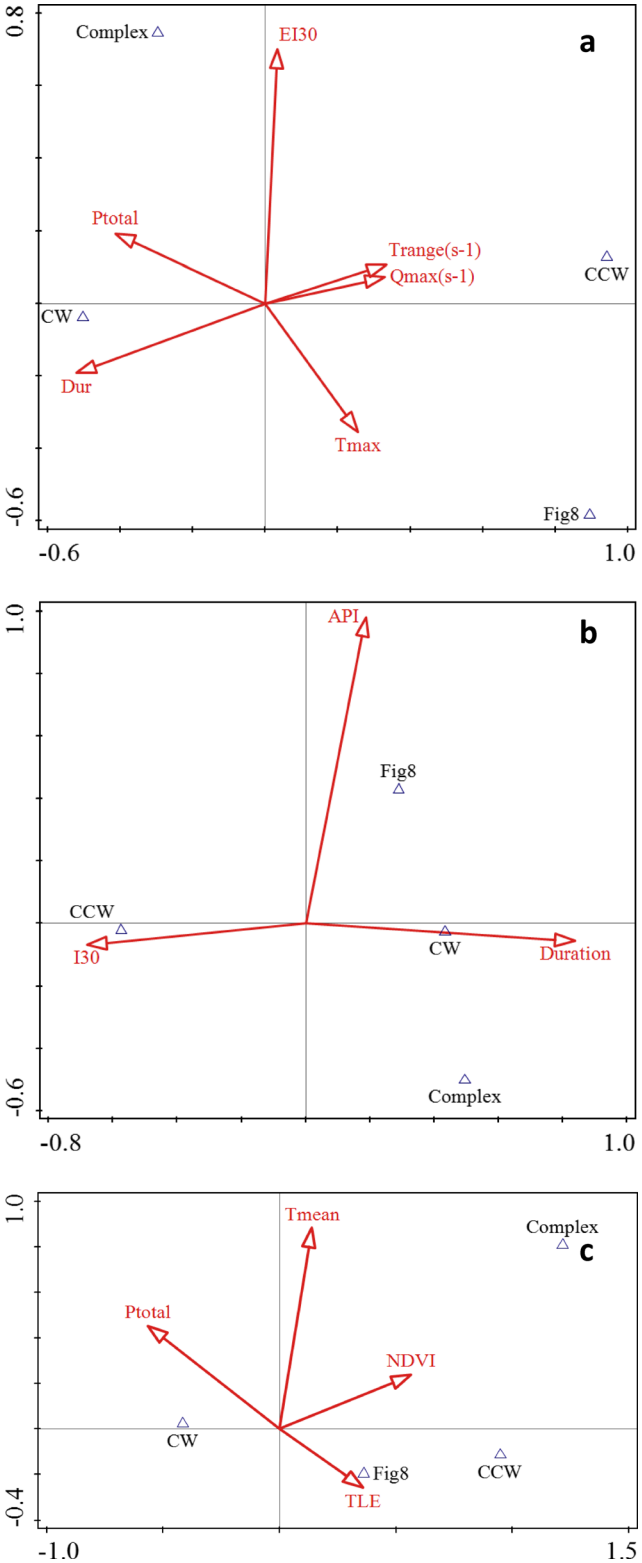

Fig. 5 Chart results of canonical variate analysis **a** Latxaga; **b** La Tejería; and **c** Oskotz

In Oskotz, the first canonical discriminant function (a1) explained 80.8% of the variance and was most loaded NDVI, P_{total} and T_{LE}. For this reason, a1 is not representative

Table 6 Results of the canonical variate analysis

Canonical variate analysis: Latxaga			Canonical variate analysis: Tejeria			Canonical variate analysis: Oskotz		
Discriminant axes summary:			Discriminant axes summary:			Discriminant axes summary:		
Statistic	Axe 1	Axe 2	Statistic	Axe 1	Axe 2	Statistic	Axe 1	Axe 2
Eigenvalue	0.46	0.05	Eigenvalue	0.25	0.07	Eigenvalue	0.36	0.03
Percent variance	85.5%	95.0%	Percent variance	84.4%	99.0%	Percent variance	90.6	98.5

of specifically discharge nor precipitation variables. An ANOVA confirmed that NDVI was differentiated between all event types ($p = 4.48e-8$) and a post hoc Tukey test indicated that the only insignificant variation in NDVI existed between CCW and Fig-8 events. P_{total} was greater for CW than CCW events, ($p = 1.21e-9$). T_{LE} was significantly longer for CCW than CW events ($p = 6.77e-5$). The second discriminant function (a2) correlated with the $I_{60,}$ EI_{30} and T_{mean} and indicated the importance of rainfall intensity and rainfall erosivity in this catchment. An event could have contained just one extra turbidity peak and become a figure-of-eight or could have contained an oscillating turbidity time series and ended up as a complex event. In both cases, high rainfall intensity was present. Figure-of-eight and CCW events tended to occur after more time since the last hydrological event as indicated by the event centroid locations relative to the arrow of T_{LE}. T_{LE} was longer for CCW than CW events ($p = 6.77e-5$). ANOVA and post hoc Tukey tests confirmed that event Duration was also longer for CW than for CCW as well as Fig-8 events ($p = 6.71e-05$).

3.4 Discharge and differences in magnitude of suspended sediment export

With the exception of the Latxaga catchment, the sign of event HI did not influence the magnitude of turbidity measured at the catchment outlet. Event turbidity mean (T_{mean}) during a runoff event was considered the best available proxy measure of suspended sediment concentration. A two-sample heterogeneous t-test confirmed that T_{mean} from Latxaga was greater for events with a negative HI than for events with a positive HI ($p = 0.05$). It has previously been reported that annual sediment concentration is three times higher and annual sediment yield was six times higher in La Tejería than in Latxaga (Casalí et al. 2008). It is thus interesting to note that the T_{mean} in La Tejería for CW events was four times that of Latxaga. However, this was less pronounced for CCW events as T_{mean} in La Tejería was only 2.7 times greater than that of Latxaga. CW events which occurred in winter and spring accounted for most of the suspended sediment which was exported during the study in these two catchments.

Channel base flow conditions and the event timing relative to previous events exerted major controls on event type outcome in Latxaga, but this affect was less pronounced in the other two catchments. Graphical analysis of a multi-event hydrograph and turbidity time-series showed that CCW events tended to occur on the recession curve of larger events while CW events tended to occur under very low base flow conditions, or on the rising limb of larger events (Fig. 6). Results of a one-tailed, heterogeneous variance *t* test indicated that positive HI events occurred under lower beginning base flow (Q_b) conditions than events with negative average HI values ($p = 0.02$). Q_b showed no significant variation between event type in either La Tejería or Oskotz.

4 Discussion

4.1 Implications of event classification algorithm

Analysis of the results confirmed that the event categorisation algorithm performed well. However, one inconsistency in the

Table 7 Results of ANOVA showing differences in mean values of event storm variables

Catchment	Latxaga					La Tejeria					Oskotz				
	CW	CCW	Fig8	Complex	*p*	CW	CCW	Fig8	Complex	p	CW	CCW	Fig8	Complex	p
Ptotal	16.74	10.18	8.14	24.20	2.90E-03	14.51	12.63	13.91	18.73	–	23.48	10.22	14.98	9.25	1.21E-09
Duration	36.09	23.62	26.33	35.38	3.14E-05	24.95	15.96	22.93	28.50	3.95E-06	46.83	32.31	34.38	41.17	6.72E-05
P_{06}						2.59	4.58	3.20	3.09	2.93E-02					
I30						3.84	6.81	3.20	2.61	1.67E-03					
$Q_{max(s-1)}$	150.45	223.42	179.13	138.68	2.95E-02										
$T_{range(s-1)}$	469.92	832.48	483.73	151.54	4.20E-03										
NDVI											166.46	179.23	217.88	270.85	4.49E-08

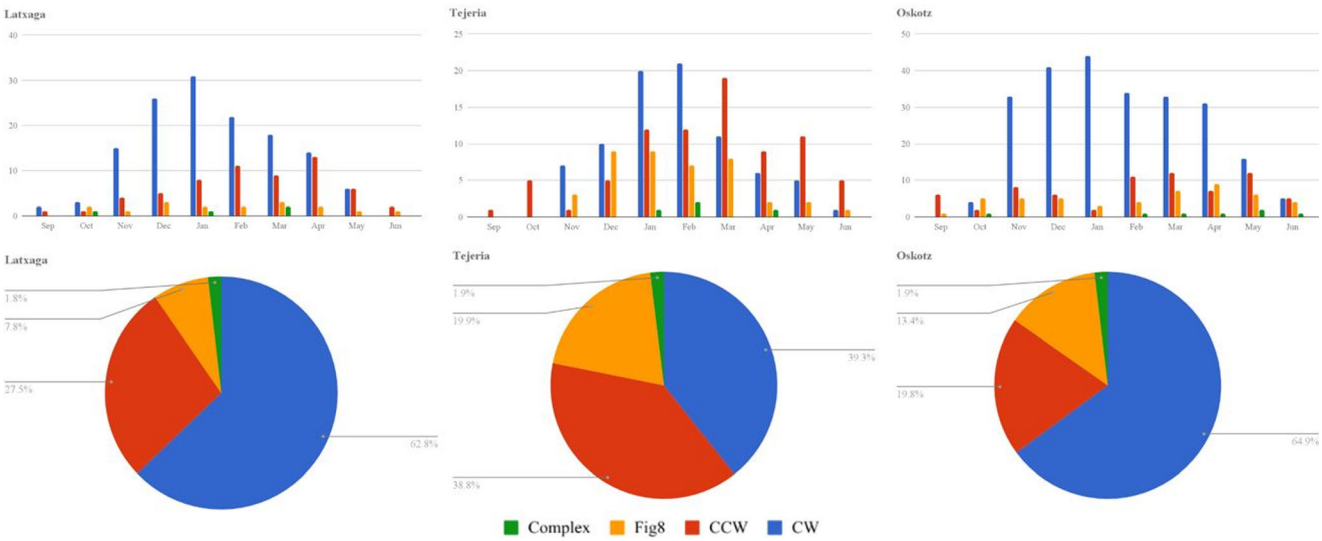

Fig. 6 Hysteresis type frequency: Number of occurrences of hysteresis on a monthly (top) and total (bottom) basis

algorithm's logic was identified: figure-of-eight events were originally defined as only having one switch in the sign of HI during the event. This meant that some events that are from a manual check are clearly figure eight events should have been categorised as complex. Despite the sign of HI switching twice, the end-of-storm jump in either the discharge or turbidity—the cause of the sign switch—directions did not cause the hysteresis curve to intersect itself. In general, the hysteresis analysis method was highly sensitive to small scale fluctuations in the time series because the min-max normalisation procedure ensured that the relative shape of the curves remained intact (Lloyd et al. 2015). This allowed the grouping algorithm to capture subtle differences in the time-to-peaks between the curves. This was especially important because the two curves were often in very close proximity. Hysteresis analysis plus event type categorisation in this regard provided extra analytical benefits to hydrological and sedimentological studies (Seeger et al. 2004).

4.2 Explanation of event type distribution

With the exception of very large runoff events, sediment supply in all catchments for CW events was confined to the channel itself, or to the areas directly adjacent to the channel. Complex and figure-of-eight events were exceptions. Heidel (1956) stated that this kind of sediment supply is characteristic for catchments with small streams, i.e. headwaters or catchments with a dense drainage pattern. This is in line with the findings of Einstein (1943), stating that suspended sediments and thus suspended sediment peaks normally travel with flow velocity, where maximum discharge peaks travel with the considerably faster wave velocity. The difference between both is less pronounced in smaller catchments due to the shorter travel distances, resulting is smaller differences in response time. The dominant presence of CW hysteresis in Latxaga and Oskotz is likely explained by the increased catchment morphological complexity and vegetative features of these two catchments. The steeper average channel gradients of La Tejería, in combination with a lower stream density and lack of channel vegetation, leads to a more erosive flow. Or, the more erosive flow in La Tejería created steeper channel gradients and a lack of channel vegetation and subsequent high occurrence of bank failures, especially in the latest stages of the rainfall event, also supports the highest importance of counter-clockwise loops in La Tejeria (Fig. 7). Subsequently, suspended sediment in La Tejería had little change for in-stream deposition because of the too high flow velocities in relation with the grain size distribution of the sediments. This is in line with the fact that La Tejería shows much higher sediment yields, compared to Latxaga, so in-stream sediment storage seems to play a crucial role. In addition, the morphological and topographic differences between watersheds, La Tejería shows a more circular shaped (see shape factor and Gravelius Index, Table 1), with a smoother topography and a higher general slope gradient of the stream channels than those of the Latxaga watershed. The circular shape (illustrated also by the shape factor (K_f, Table 1)), flatter topography and higher average slope gradient of stream channels causes more efficient runoff generation which higher peak discharges at the outlet. Moreover, the more complex topography, with a floodplain and more abundant riparian vegetation in Latxaga, favours sedimentation within the catchment before reaching the outlet. The effect of the catchment complexity on the amount of sediment yield was also shown by a modelling effort by Casalí et al. (2008) who found that Latxaga's elongated shape reduced the sediment yield three to five times compared to the rounded La Tejeria catchment.

Fig. 7 Landscapes of Latxaga (**a**): complex morphology, riparian vegetation and La Tejeria (**b**): smooth, little riparian vegetation and bank failures

The figure-of-eight and complex hysteresis events indicate the initiation of sediment connectivity between the sampling location and remote sources of sediment, i.e. non-channel of up-catchment sources. In both Latxaga and La Tejería, figure-of-eight hysteresis events that started as CW events tended to occur under low-flow conditions, whereas figure-of-eight hysteresis events that started as CCW tended to occur under higher flow conditions. In La Tejería has steeper average channel gradients and lack of channel vegetation. Therefore, the erosion processes can be explained by late-stage river bank collapses, as well as a combination of saturation excess and infiltration excess overland flow, which contains freshly mobilised sediment due to high rainfall intensities. In this La Tejería catchment, oscillations in turbidity during the discharge recession implicate up-catchment sediment connectivity or slow responding in-stream sediment additions. Once the hillslope sediments reached the outlet, the turbidity increased while the channel discharge already was in the after-peak recession. Seeger et al. (2004) showed that when the rainfall intensity decreases, the generation of Hortonian overland flow will subside. In La Tejería however, the decline in the suspended sediment concentration was faster than the decline in discharge. As a result, without a high API, CCW events in La Tejería tended to remain CCW rather than converting to figure-of-eight or complex events.

4.3 Hysteresis analysis as a signal of sediment and hydrological connectivity

Hysteresis loops capture the discrepancy between discharge and suspended sediment concentration during runoff events (Gao and Josefson 2012). This analysis of three small catchments in Northwest Spain revealed patterns which could link discharge and suspended sediment concentrations as products of non-linearity in hydrological connections via overland flow (runoff) and associated sediment connections due to sediment entrainment (Bracken et al. 2015; Keesstra et al. 2018). It was found that spatial and temporal variability of erosion, transport and sedimentation were continuously changing due to variation in catchment and channel state before and during a storm event, which is in line with similar findings by Cooper et al. (2012). The variation in transport times between water to channel outlet were explained by variations in hydrological and sediment connectivity (Bracken and Croke 2007; Bracken et al. 2015; Parsons et al. 2015; Poeppl et al. 2017). These types of connectivity could be linked to complex landscape and channel morphology and could also be linked to the feedback mechanisms between sediment source locations, transport pathways and sinks (Heckmann and Vericat 2018), such as the co-evolution of riparian vegetation and floodplain sedimentation. The forested Oskotz catchment showed decreased sediment connectivity between hillslopes and the channel. However, because of tree cutting, bare land patches were formed. These act as sediment sources from which overland flow at intense rain storms can develop. This overland flow brings sediments to the channel (Casalí et al. 2010). Finally, La Tejería with its steeper gradients, deeper channel incision and non-vegetated channel bed (Fig. 7), displayed much more surface hydrological (runoff) as well as sediment connectivity. The overall sediment yield was three to five times higher (Casalí et al. 2010) and this catchment displayed a more balanced HI distribution between CW and CCW events.

Therefore, we conclude that a hysteresis analysis can be a good method for assessing sediment connectivity on small catchment scale. Because we have good knowledge of the catchment dynamics in these systems, from other studies conducted in these catchments (Casalí et al. 2008, 2010, 2012; Masselink et al. 2016, 2017) it is possible to link the catchment complexity to a majority of CW loops; and high sediment yields and low complexity to a more mixed CCW and CW system. Even though this study did not include an explicit analysis of the hillslope erosion processes, it was possible to capture the emergent nature of the sediment transport through continuous and systematic classification of differences in water and sediment delivery at the catchment outlet. The extensive use of data on the initial hydrological state of a catchment agrees with Faulkner's (2008) definition of sediment

connectivity, which states that sediment connectivity incorporates the integrated status of a system within the catchment.

5 Conclusions

The use of hysteresis analysis on 10 min hydrological and turbidity data in this study allowed for a detailed analysis of sediment and fine-grained sediment transport to streams located in three contrasting morphological, hydrogeological and landscape character catchments under event flow conditions. The quantitative method developed in this paper includes all available data, and allowed for the first time, rain storms to be automatically classified based on a range of HI distributions throughout the event for all events in the rainfall record of in this case up to ##years. The data on catchments initial state and previous precipitation events has also proven to provide useful data with which the connectivity analysis could be compared and validated.

In the Spanish catchments where the tool was tested clockwise, hysteresis was more dominant in the more disconnected catchments of Latxaga and Oskotz. Counter-clockwise hysteresis occurred equally as much as clockwise hysteresis in La Tejería, with its circular shape and relatively deeply incised channel. Complex event types (figure-of-eight; complex) in all catchments were the result of runoff and sediment connectivity between the channel and hillslopes.

Hysteresis analysis is a valuable tool for assessing event sediment transport behaviours and provided a robust method for comparing how catchments function to generate and transport sediment as well as to assess the state of sediment connectivity. It has further shown that these differences sediment transport times result emerge over time differently due to catchment morphological complexity, distribution and intensity of vegetation and topographical factors. Knowledge from this type of analysis can lead to further application of the algorithm herein described, in order to identify sediment source locations, transport pathways and sink locations. It can therefore be of use to catchment managers who are seeking robust, cost effective and precise ways to mitigate excess sediment losses on and between fields. Including all available data in terms of water and sediment discharge makes the technique more reliable than most other studies using hysteresis, where an only a selection of the storms is evaluated.

Acknowledgements This study was supported by the effective network that was created in COST Action CONNECTEUR (ES1306, Connecting European Connectivity Research). Furthermore, we would like to acknowledge the support of the Research Project CGL2015-64284-C2-1-R, founded by the Spanish Ministry of Economy and Competitiveness.

References

Aich V, Liersch S, Vetter T, Huang S, Tecklenburg J, Hoffmann P, Koch H, Fournet S, Krysanova V, Müller E, Hattermann FF (2014) Comparing impacts of climate change on streamflow in four large African river basins. Hydrol Earth Syst Sci 18(4):1305–1321

Bendjoudi H, Hubert P (2002) Le coefficient de compacité de Gravelius: analyse critique d'un indice de forme des bassins versants. Hydrological sciences journal, 47(6):921–930

Bilotta GS, Brazier RE (2008) Understanding the influence of suspended solids on water quality and aquatic biota. Water Res 42:2849–2861

Bird G, Brewer PA, Macklin MG, Nikolova M, Kotsev T, Mollov M, Swain C (2010) Quantifying sediment-associated metal dispersal using Pb isotopes: application of binary and multivariate mixing models at the catchment-scale. Environ Pollut 158(6):2158–2169

Bracken LJ, Croke J (2007) The concept of hydrological connectivity and its contribution to understanding runofff-dominated geomorphic systems. Hydrol Process 21:1749–1763

Bracken LJ, Turnbull L, Wainwright J, Bogaart P (2015) Sediment connectivity: a framework for understanding sediment transfer at multiple scales. Earth Surf Process Landf 40:177–188

Brown LC, Foster GR (1987) Storm erosivity using idealized intensity distributions. Trans ASAE 30:379–386

Casalí J, Gastesi R, Álvarez-Mozos J, De Santisteban LM, de Lersundi JDV, Giménez R, López JJ (2008) Runoff, erosion, and water quality of agricultural watersheds in central Navarre (Spain). Agric Water Manag 95:1111–1128

Casalí J, Giménez R, Díez J, Álvarez-Mozos J, de Lersundi JDV, Goñi M, López J (2010) Sediment production and water quality of watersheds with contrasting land use in Navarre (Spain). Agric Water Manag 97:1683–1694

Casalí J, Loizu J, Campo MA, De Santisteban LM, Álvarez-Mozos (2012) Runoff, erosion and water wuality of agricultural watersheds in central Navarre (Spain). Agric Water Manag 110:1–8

Cerdà A, Keesstra SD, Rodrigo-Comino J, Novara A, Pereira P, Brevik E, Giménez-Morera A, Fernández-Raga M, Pulido M, di Prima S, Jordán A (2017) Runoff initiation, soil detachment and connectivity are enhanced as a consequence of vineyards plantations. J Environ Manag 202:268–275

Cerdan O, et al. (2010) Rates and spatial variations of soil erosion in Europe: a study based on erosion plot data. Geomorphology, 122. Jg., Nr. 1-2, S. 167–177

Cerro C, Bech J, Codina B, Lorente J (1998) Modeling rain erosivity using disdrometric techniques. Soil Sci Soc Am J 62:731–735

Cooper JR, Wainwright J, Parsons AJ, Onda Y, Fukuwara T, Obana, E, Hargrave, GH (2012) A new approach for simulating the redistribution of soil particles by water erosion: a marker-in-cell model. J Geophys Res Earth Surf 117(F4). https://doi.org/10.1029/2012JF002499

Dash J, Mathur A, Foody GM, Curran PJ, Chipman JW, Lillesand TM (2007) Land cover classification using multi-temporal MERIS vegetation indices. Int J Remote Sens 28:1137–1159

Eckhardt K (2005) How to construct recursive digital filters for baseflow separation. Hydrol Process 19:507–515

Einstein HA (1943) Flow on a movable bed. Proc Hydraulic Conf Univ of Iowa Bulletin, pp 333–341

Faulkner H (2008) Connectivity as a crucial determinant of badland morphology and evolution. Geomorphology 100:91–103

Gao P, Josefson M (2012) Temporal variations of suspended sediment transport in Oneida Creek watershed, central New York. J Hydrol 426-427:17–27

Gao P, Pasternack G (2007) Dynamics of suspended sediment transport at field-scale drain channels of irrigation-dominated watersheds in the Sonoran Desert, southeastern California. Hydrol Process 21:2081–2092

García-Ruiz JM, Nadal-Romero E, Lana-Renault N, Beguería S (2013) Erosion in Mediterranean landscapes: changes and future challenges. Geomorphology 198:20–36

Gentile F, Bisantino T, Corbino R, Milillo F, Romano G, Liuzzi GT (2010) Monitoring and analysis of suspended sediment transport dynamics in the Carapelle torrent (southern Italy). Catena 80:1–8

Heckmann T, Vericat D (2018) Computing spatially distributed sediment delivery ratios: inferring functional sediment connectivity from repeat high-resolution digital elevation models. Earth Surf Process Landf 43:1547–1554

Heidel SG (1956) The progressive lag of sediment concentration with flood waves. EOS 37:56–66

Jansson MB (2002) Determining sediment source areas in a tropical river basin, Costa Rica. Catena 47:63–84

Keesstra SD, van Dam O, Verstraeten G, van Huissteden J (2009) Changing sediment dynamics due to natural reforestation in the Dragonja catchment, SW Slovenia. Catena 78:60–71

Keesstra S, Nunes JP, Saco P, Parsons T, Poeppl R, Masselink R, Cerdà A (2018) The way forward: can connectivity be useful to design better measuring and modelling schemes for water and sediment dynamics? Sci Total Environ 644:1557–1572

Kjelland ME, Woodley CM, Swannack TM, Smith DL (2015) A review of the potential effects of suspended sediment on fishes: potential dredging-related physiological, behavioral, and transgenerational implications. Environ Syst Decis 35:334–350

Klein M (1984) Anti clockwise hysteresis in suspended sediment concentration during individual storms: Holbeck Catchment; Yorkshire, England. Catena 11:251–257

Langlois JL, Johnson DW, Mehuys GR (2005) Suspended sediment dynamics associated with snowmelt runoff in a small mountain stream of Lake Tahoe (Nevada). Hydrol Process 19:3569–3580

Lawler DM, Petts GE, Foster ID, Harper S (2006) Turbidity dynamics during spring storm events in an urban headwater river system: the Upper Tame, West Midlands, UK. Sci Total Environ 360:109–126

Linsley RK, Kohler MA (1951) Variations in storm rainfall over small areas. Eos, Transactions Am. Geophys Union 32:245–250

Lloyd CEM, Freer JE, Johnes PJ, Collins AL (2015) Testing an improved index for analysing storm nutrient hysteresis. Hydrology and Earth System Sciences Discussions, 12(8):7875–7892

Lloyd CEM, Freer JE, Johnes PJ, Collins AL (2016) Using hysteresis analysis of high resolution water quality monitoring data, including uncertainty, to infer controls on nutrient and sediment transfer in catchments. Sci Total Environ 543:388–404

López-Tarazón JA, Batalla RJ, Vericat D, Francke T (2009) Suspended sediment transport in a highly erodible catchment: the River Isábena (Southern Pyrenees). Geomorphology 109:210–221

Mano V, Nemery J, Belleudy P, Poirel A (2009) Assessment of suspended sediment transport in four alpine watersheds (France): influence of the climatic regime. Hydrol Process 23(5):777–792

Masselink RJH, Keesstra SD, Temme AJAM, Seeger M, Giménez R, Casalí J (2016) Modelling discharge and sediment yield at catchment scale using connectivity components. Land Degrad Dev 27:933–945

Masselink RJH, Temme AJAM, Giménez R, Casalí J, Keesstra SD (2017) Assessing hillslope-channel connectivity in an agricultural catchment using rare-earth oxide tracers and random forests models | Valorando la conectividad ladera-cauce en una cuenca agrícola, utilizando óxidos de tierras raras como trazadores y modelos de Cuad. Investig Geogr 43:19–39

Monsalve Sáenz, G. (1999). Hidrología en la Ingeniería. Alfaomega, Colombia

Morgan RPC (2005) Soil erosion and conservation. Longman Group Limited, UK, pp 63–74

Nathan RJ, McMahon TA (1990) Evaluation of automated techniques for base flow and recession analyses. Water Resour Res 26:1465–1473

Owens PN, Walling DE (2002) The phosphorus content of fluvial sediment in rural and industrialized river basins. Water Res 36:685–701

Parsons AJ, Wainwright J, Brazier RE, Powell DM (2006) Is sediment delivery a fallacy? Earth Surf Process Landf 31:1325–1328

Parsons AJ, Bracken L, Poeppl RE, Wainwright J, Keesstra SD (2015) Introduction to special issue on connectivity in water and sediment dynamics. Earth Surf Process Landf 40:1275–1277

Poeppl RE, Keesstra SD, Maroulis J (2017) A conceptual connectivity framework for understanding geomorphic change in human-impacted fluvial systems. Geomorphology 277:237–250

Regüés D, Guàrdia R, Gallart F (2000) Geomorphic agents versus vegetation spreading as causes of badland occurence in a Mediterranean subhumid mountainous area. Catena 40:173–187

Roehl JE (1962) Sediment source areas, delivery ratios and influencing morphological factors. Int Assoc Hydrol Sci Publ 59:202–213

Rovira A, Batalla RJ (2006) Temporal distribution of suspended sediment transport in a Mediterranean basin: the lower Tordera (NE Spain). Geomorphology 79:58–71

Seeger M, Errea MP, Begueria S, Arnáez J, Marti C, García-Ruiz JM (2004) Catchment soil moisture and rainfall characteristics as determinant factors for discharge/suspended sediment hysteretic loops in a small headwater catchment in the Spanish Pyrenees. J Hydrol 288: 299–311

Sherriff SC, Rowan JS, Melland AR, Jordan P, Fenton O, Huallachain DO (2015) Investigating suspended sediment dynamics in contrasting agricultural catchments using ex situ tubidity-based suspended sediment monitoring. Hydrol Earth Syst Sci 19:3349–3363

Sith R, Yamamoto T, Watanabe A, Nakamura T, Nadaoka K (2017) Analysis of red soil sediment yield in a small agricultural watershed in Ishigaki Island, Japan, using long–term and high resolution monitoring data. Environ Process 4:333–354

Sloto RA, Crouse MY (1996) HYSEP, a computer program for streamflow hydrograph separation and analysis. US Department of the Interior, US Geological Survey 96(4040):96

Smith HG, Dragovich D (2009) Interpreting sediment delivery processes using suspended sediment-discharge hysteresis patterns from nested upland catchments, south-eastern Australia. Hydrol Process 23: 2415–2426

Song Y, Ji J, Yang Z, Yuan X, Mao C, Frost RL, Ayoko GA (2011) Geochemical behavior assessment and apportionment of heavy metal contaminants in the bottom sediments of lower reach of Changjiang River. Catena 85:73–81

Stubblefield AP, Reuter JE, Dahlgren RA, Goldman CR (2007) Use of turbidometry to characterize suspended sediment and phosphorus fluxes in the Lake Tahoe basin, California, USA. Hydrol Process 21:281–291

Ter Braak CJF, Smilauer P (2012) CANOCO. Biometris, Wageningen, p 5

Wainwright J, Turnbull L, Ibrahim TG, Lexartza-Artza I, Thornton SF, Brazier RE (2011) Linking environmental regimes, space and time: interpretations of structural and functional connectivity. Geomorphology 126:387–404

Williams GP (1989) Sediment concentration versus water discharge during single hydrologic events in rivers. Journal of Hydrology, 111(1-4):89–106

Wotling G, Bouvier CH (2002) Impact of urbanization on suspended sediment and organic matter fluxes from small catchments in Tahiti. Hydrol Process 16:1745–1756

Zabaleta A, Martínez M, Uriarte JA, Antigüedad I (2007) Factors controlling suspended sediment yield during runoff events in small headwater catchments of the Basque Country. Catena 71:179–190

Ziegler AD, Benner SG, Tantasirin C, Wood SH, Sutherland RA, Sidle RC, Jachowski N, Nullet M, Xi LX, Snidvongs A, Giambelluca TW, Fox JF (2014) Turbidity-based sediment monitoring in northern Thailand: hysteresis, variability, and uncertainty. J Hydrol 519: 2020–2039